CROP HEIGHT MONITORING USING A CONSUMER GRADE CAMERA AND UAV TECHNOLOGY

D. Belton [a], P. Helmholz [a*], J. Long [a], A. Zerihun [b]

[a]School of Earth and Planetary Sciences, Curtin University, Perth WA 6845, Australia –
(D.Belton, Petra.Helmholz, John.Long)@curtin.edu.au

[b]Centre for Crop and Disease Management, School of Molecular and Life Sciences, Curtin University, Perth WA 6845, Australia – a.zerihun@curtin.edu.au

*Corresponding author

KEY WORDS:

Crop Monitoring, Crop Surface Model, Digital Surface Model, Low Cost Sensor System, Unmanned Aerial Vehicles, UAV in Agriculture

ZUSAMMENFASSUNG:

Jüngsten Fortschritte bei der Erfassung von Bildern mit hoher Auflösung durch unbemannte Luftfahrzeuge (Unmanned Aerial Vehicles, UAV) haben das Potenzial dieser Technologie für einen breiten Anwendungsbereich aufgezeigt, einschließlich der Untersuchung der Auswirkungen verschiedener externer Reize bei der Überwachung von Umgebungs- und Strukturvariablen. In diesem Artikel zeigen wir die Anwendung der UAV-Technologie zur Überwachung und Modellierung von Getreidehöhen, um quantitative Getreidewachstumshöhen bereitzustellen und die Fernerkundungs- und photogrammetrischen Fähigkeiten der Technologie für die Landwirtschaft zu demonstrieren. Diese Studie wurde in einem Feldversuch mit einer Kombination von sechs Weizensorten und drei verschiedenen Pilzbehandlungen durchgeführt. Die UAV-Bilder des Feldversuchsgeländes wurden während der gesamten Ernteentwicklung fünfmal aufgenommen. Diese Bilder wurden verwendet, um digitale Oberflächenmodelle (Digital Surface Models - DSMs) zu erstellen, aus denen Getreideoberflächenmodelle (Crop Surface Models - CSMs) für die Versuchsflächen extrahiert wurden. Die Erntehöhen werden aus den photogrammetrisch abgeleiteten CSMs geschätzt und mit den Referenzhöhen verglichen, die mit dem Global Navigation Satellite System (GNSS) von Real-Time Kinematic (RTK) zur Validierung der CSMs erfasst wurden. Darüber hinaus werden Unterschiede im Pflanzenwachstum zwischen den Sorten analysiert und die Korrelation der Getreidehöhe mit dem Getreideertrag sowie mit unabhängig geschätzten Vegetationsindizes werden ausgewertet. Diese Auswertungen zeigen, dass die Technologie geeignet ist (mit einem durchschnittlichen Bias-Bereich von 2 bis 10 cm in Abhängigkeit von den

Windverhältnissen in Bezug auf die GNSS-Höhe) und das Potenzial zur quantitativen und qualitativen Überwachung der Getreidehöhe und des Wachstums vorhanden ist.

ABSTRACT:

Recent advances in the ability to capture high spatial resolution images by Unmanned Aerial Vehicles (UAVs) have shown the potential of this technology for a wide range of application including exploring effects of different external stimuli when monitoring environmental and structural variables. In this paper, we show the application of UAV technology for crop height monitoring and modelling to provide quantitative crop growth data and demonstrate the remote sensing and photogrammetric capabilities of the technology to the farming industry. This study was carried out in a field trial involving a combination of six wheat varieties and three different fungicide treatments. UAV imagery of the field trial site was captured on five occasions throughout the crop development. These were used to create digital surface models (DSMs) from which crop surface models (CSMs) were extracted for the cropped areas. Crop heights are estimated from the photogrammetric derived CSMs and are compared against the reference heights captured using Real-Time Kinematic (RTK) Global Navigation Satellite System (GNSS) to validate the CSMs. Furthermore, crop growth differences among varieties are analysed; and crop height correlations with grain yield as well as with independently estimated vegetation indices are evaluated. These evaluations show that the technology is suitable (with average bias range 2-10 cm depending on wind conditions relative to GNSS height), and has potential, for quantitative and qualitative monitoring of canopy and/or crop height and growth.

1. INTRODUCTION

The use of photogrammetry and airborne laser scanning is a common method in remote sensing for modelling canopy surfaces and attributes, as it enables the extraction and separation of the canopy layers, and attributes such as heights, density and health for applications in forestry and vegetation monitoring (St-Onge et al., 2008). Monitoring attributes of crops throughout their developmental phases is an important prerequisite for precision agriculture (Mulla, 2013; Laudien and Bareth, 2006). Information gained from monitoring crop health can be used to guide and develop efficient crop management strategies, and help improve accuracies of crop yield predictions. Such knowledge can be obtained from different crop parameters, and include variables such as plant height, biomass, soil and plant nitrogen levels, along with others (Goyne et al., 1996).

One technology that is gaining increasing use in measuring or analysing these attributes is UAV Photogrammetry. The terminology *UAV Photogrammetry* (Eisenbeiss, 2008) refers to a photogrammetric measurement platform which operates via remote control either fully autonomously or semi-autonomously and without the need for a pilot to occupy the aircraft. The platform is equipped with a photogrammetric measurement system which includes either small or medium format cameras, or different sensor types such as thermal or infrared camera systems, airborne LiDAR system or a combination of multiple measurement systems. UAVs can also house GNSS receivers and orientation sensors which can be used in local or global coordinate systems. However, UAVs, especially low-cost UAVs, are extremely limited by the payload of the sensor or camera in terms of weight and dimension, and the endurance is often a compromise between flight time and payload capacity. Common low-weight sensors like small or medium consumer grade cameras are limited by their ability to capture multispectral data unless they have been modified. Low-cost sensors are also normally less stable than high-end sensors, and may cause a reduction in image quality and data resolution.

Nevertheless, multi-faceted developments in technologies have led to integrated system that can deliver accurate results. This has been made possible due to advances in efficient data capture, miniaturisation and the lowering of cost of image sensors, as well as parallel developments in UAV hardware such as navigation systems, control systems and motors. However, the execution of efficient data capture and processing the images still requires rigorous planning and understanding, and a highly redundant data capture campaign to improve data quality. The increasing ability and availability of sensors means that it is becoming increasingly capable in identifying and quantifying

attributes of a desired target – plant, structure, etc. Also due to the low cost and ease of deployment, it allows for a high density data capture not just in the spatial domain, but in the temporal domain, allowing more detailed longitudinal analysis and modelling.

In this paper, the measurement of crop height and estimation of temporal changes in crop height of six different wheat varieties is examined using a consumer grade camera and a UAV as a method of data capture. With different epochs of data capture, focus is made on the generation of CSM from UAV-imagery to evaluate whether such data obtained from low-cost sensors can be used for monitoring and/or resolving crop height differences as well as yield prediction among wheat varieties with known variations in height. The CSMs are validated through GNSS RTK data acquired in parallel.

The paper is structured as follows: Section 2 reviews UAV systems and research in the field of photogrammetry with an agricultural focus. Sections 3 and 4 focus on the background processes and information used throughout the study, along with descriptions of the procedure used for automated photogrammetric data acquisition using UAV systems and the processing of the aerial images. Section 5 covers analyses of the UAV data captured, with an emphasis on four tests conducted to evaluate the usefulness and accuracy of all generated data, along with results and discussion. These included assessment of the photogrammetry results, comparison of the extracted heights to GNSS data, comparison of the crop heights in capture epochs to the ground surface, and the correlation between extracted heights and the crop yield and NDVI (normalised difference vegetation index) values. In Section 6, the conclusions are drawn supplemented with an outlook to future applications.

2. RELATED WORK

Digital surface models generated from UAV-borne sensor data capture are becoming useful tools in many applications such as rapid mapping for disasters (Batzdorfer et al., 2017), heritage documentation (Chiabrando and Losè, 2017), building inspection (Duarte et al., 2017), power line corridors mapping (Maurer et al., 2017), tree crown structure mapping (Hese and Behrendt, 2017), wetland species mapping and coastal environmental mapping (Taddia et al., 2017). For all these applications UAVs are used to collect data at very high spatial and/or temporal resolutions. The requirement on the accuracy of the spatial data and the resolution of the temporal aspects vary depending on the application. The assessment of the spatial accuracy of UAV derived data and products depends on a number of contributing factors such as the camera specifications (Mostafa,

2017), component and method used for geo-referencing (Stöcker et al., 2017; Rehak and Skaloud, 2017), the mapping system, e.g., fixed wing vs rotary blade (Boon et al, 2017), the flight height and number of control points. For agronomic applications, the Ground Sampling Distance (GSD) (pixel resolution) as a measure for the spatial resolution is usually within the low centimetre range (Bendig et al., 2013) and is found to be sufficient. Currently, the common method of plant height determination in agronomy involves manual, graduated (telescopic) poles, rulers or measuring tapes which are only good for point measurements. More recently, LiDAR has been evaluated at research scale (Shi et al., 2016; Candare et al., 2016).

Beside the temporal and the spatial resolution, the spectral resolution (number and width of spectral bands captured) is important for agronomic applications (Abbasi et al., 2010; Herrmann et al., 2010; Wang et al., 2016). However, the capture of high spectral resolution data is limited by the payload of UAV platforms, and the limited range of suitable cameras with more than four spectral bands.

Geipel et al. (2014) argue that Red, Green, Blue (RGB) imagery captured from consumer cameras provides adequate information for creating CSMs. The spectral information from the imagery also has the potential to determine crop positions and estimate site specific crop management factors such as the possibility of predicting grain yield. Geipel et al. (2014) endeavoured to (1) evaluate the suitability of UAVs for providing precision farming management strategies, and (2) determine the maximum achievable CSM detail from UAV imagery. Problems that arose during this investigation were the lack of independent reference to another height measurement technique, or a source of reference data.

Bendig et al. (2013) also created CSMs by using very high resolution imagery taken via a UAV platform. The key focus of this study was to detect differences in crop heights based on the application of different farming practices to each trial crop. The field data capture was carried out over five different periods, during the crops' most productive growth period, May to June. They established 18 Ground Control Points (GCPs) at the corners of the trial plots to provide reference and control survey information. The in-field control survey consisted of the use of a ruler placed next to the crops in three separate positions, which gave an independent check to the plant heights with a precision of 0.01 m. Bendig et al. (2013) created an individual check for the accuracy of their CSM height estimates by comparing minimum, maximum, range, mean, and standard deviation of plant height to reference data. A mean difference between the CMS and the reference values of 0.02 m was observed,

and the correlation between the reference and CSM measurements was 0.99. A problem that arose during the Bendig et al. (2013) study was the increasing height and density of the crop, which obstructed some GCPs in the captured imagery. The weather conditions also affected the use of four of the five datasets as strong winds affected the image quality and biased the results.

Sona et al. (2016) describe two multispectral surveys performed over a maize field on bare soil before sowing, and at a later time, on the crop, when the maize crop was nearly at the maximum height, just before flowering. The difficulties that arise in using automatic processing algorithms available in commercial software solutions based on Structure for Motion algorithms are analysed by Sona et al. (2016), and the corrective actions which were adopted are described. The procedures (not completely automatic) adopted to produce DSM, orthophotos and maps of spectral indices are illustrated, but were limited to a small sampling size. While initial analyses of soil classification, obtained by a joint use of aerial optical data and ground geophysical data, are presented, final conclusions about the usability of UAV for crop monitoring are not drawn.

The investigations of Nebiker et al. (2016) focused on the performance of new light-weight multispectral sensors for micro UAVs. Their experimentation focused initially on evaluating two different sensors, a high and a low cost sensor. It was shown that the values obtained from the high-end system consistently agree with the reference values with a mean difference in the order of 0.01-0.04 NDVI values. The values obtained with the low-cost system exhibited significant biases from the reference values, but exhibited a reasonable correlation with the values sampled from the high-end system. On the other hand, the low-cost sensor has a much higher image resolution (pixels/sensor), which provides a much denser data set. This formed the second focus of the study, where the higher resolution captured from the low-cost multi-spectral camera option was used to monitor the spread of diseases in different vegetable plants, where it was determined (based on these high-resolution index maps) that it was possible to monitor the propagation of the diseases. All experiments provided valuable further information on optimal times and intervals for UAV-based monitoring. However, the study did not address if the spreading of diseases/treatment of plants could be detected with index maps only or requires augmentation by geometric information such as crop heights.

In this work, we aimed to evaluate the capability of UAV technology to track temporal changes in crop heights over a growing season. This has the application of non-invasive and rapid monitoring of

crop growth responses to changes in environment and management effects. Attention is given to the generation of the CSMs and the extraction of the height information as the theory of modelling crop surfaces is a relatively new concept to the discipline of crop science. With respect to data acquisition in our experiments, we took into account experiences from previous studies in relation to the ground resolution, flight heights, image overlaps and their relation to the camera specifications.

3. METHODOLOGY

The data capture campaign was scheduled around broad growth stages (GS) of the crop to ensure adequate capture. Thus, data captures were made of the bare ground prior to crop emergence (GS00, Epoch 0), at the mid to late tillering phase (GS25-GS30, depending on variety: Epoch 1), at heading to early flowering (GS55-62: Epoch 2) and at mid-flowering to early grain-filling period (GS65-73: Epoch 3) and at haying-off stage (>GS 77, Epoch 4). The following workflow was followed for image capture and data processing.

Flight Planning: Before any data capture for the project can commence, planning for the anticipated objectives and procedures to be used in the project has to be completed with the best photogrammetric practice. This includes the flight planning for the area of interest and how additional data will be captured, such as reference GNSS observations. This ensures comparable data are captured over successive epochs in terms of context and resolution.

The flight parameters were calculated based on the targeted GSD (of 2 cm GSD), the camera model and overlap requirements (Kraus, 2007). The target 2 cm GSD was determined as compromise between getting good ground resolution and capturing images with well-defined features to allow matching and generation of a surface. Furthermore, sufficient ground control points were placed on the borders of the survey area as well as in the centre to stabilise the photogrammetric adjustment (Kraus, 2007).

Data Capturing: In order to determine how well the surface (absolute height) of the crops is modelled in the CSMs, reference data were captured using two different methods. Firstly, measurements using GNSS RTK were recorded, where two series of observations were taken, one at ground level, and one at the top of the crop canopy. GNSS RTK has a theoretical accuracy of $\pm$ 8 mm $\pm$0.5ppm horizontally and $\pm$ 15 mm $\pm$ 0.5ppm vertically for well-defined marks. The survey area was

approximately 3 km from a Standard Survey Mark (SSM), and the GNSS RTK was used to record the GCPs, with a reported absolute horizontal and vertical accuracy of 0.023 m and 0.030 m, respectively, based on the in-field measurements. The accuracy for capturing the crop surface using the GNSS RTK is not only influenced by the actual GNSS accuracy, but also by ability to pick the top point of the canopy. Crop canopy surface (absolute) heights were captured by GNSS RTK by placing the bottom of the GNSS RTK rover level to the top of the crop. Therefore, it is determined that the accuracy of crop surface height estimation with GNSS RTK is reduced to 4 cm based on empirical results from repeated assessments. Secondly, a tape measure was manually used for readings of relative crop height (height between the surface of the crop and the bare soil); it is assumed that this method has a similar accuracy to method 1 (GNSS readings). UAV data were captured over five epochs, namely, bare soil (epoch 0), three epochs during the growing phase (epochs 1-3) and a final epoch close to the harvest (epoch 4).

Data processing: Before any CSM can be created, the UAV images are processed as per the general photogrammetric workflow for processing of aerial images (Colomina and Molina, 2014). Images were processed using Agisoft PhotoScan Professional Edition Version 1.1.6. The first step is to extract feature points between images and align them with respect to each other. The next step is to identify the ground control between images to be included in the adjustment, along with the coordinates determined from RTK-GNSS. The bundle adjustment is then performed on these images and control, simultaneously solving for the Interior Orientation (IO) for the camera and the Exterior Orientation (EO) Parameters. For the IO parameters, this includes the focal length, principal point offset and radial lens distortions for each camera and for each individual epoch. For the EO parameters, this included the position (*X, Y, Z*) and orientation (*Omega, Phi, Kappa*) of all images are calculated. From this information, the creation of 3D outputs (such as the 3D coordinates of relative feature points, dense point matching, surface models) can now be performed.

CSM creation: For crop surface modelling, dense point clouds were generated first using the dense image matching in Agisoft Photoscan. A mesh was then constructed in order to represent the surface model as a continuous surface to allow for modelling and interpolation of the DSM. From the DSM, the areas corresponding to the crop plots were isolated to extract the CSM. This was done through the use of GNSS RTK point surveyed at the corner of each plot, and verified against the height discontinuities in the DSM as the crops grew. Multiple CSMs were generated with every epoch of images captured throughout the project. The CSMs from the different epochs were overlaid across

one another, and the information extracted was used to determine the growth of the crops. Gross outliers were identified by visual inspection. Outlier detection was performed in this step to ensure the removal of spikes and nonsensical data from the CSM (for example data below the ground surface).

Evaluation of crop heights per epoch: The CSM absolute heights extracted at the GNSS locations from each epoch are compared to the respective reference GNSS RTK absolute heights. A two-tailed two sample t-test procedure (sample variances were within 1 to 3% of each other at each epoch) is applied to evaluate differences between the methods. The null hypothesis being evaluated is that the crop height estimates generated from the CSM are equal to those from the reference GNSS RTK heights. Differences between the two methods estimates are declared significant if the probability of observing a difference greater than that observed is 5% or less. Comparisons were based on absolute heights unless specified otherwise.

Evaluation of crop height between epochs: Absolute crop heights extracted from CSM of each epoch were presented graphically to examine if the heights captured followed the expected patterns during the course of crop development.

4. STUDY AREA AND DATA CAPTURING

The study site (31.731°S, 116.698°E) was located near Northam, in the wheat belt of Western Australia. The trial contained a total of 114 plots. Fifty four of these plots were used to evaluate effects of three fungicide application timings for control of yellow spot disease in six different wheat varieties. The fungicide application timings (treatments) were: untreated control, Prosaro® spray at Zadock Growth Stage 31 (GS31) and spray at GS31 followed by GS39 (GS31 fb GS39). These three treatments (control, GS31, GS31 fb GS39) where applied to all six varieties of wheat resulting in a total of 18 treatments. The trial plots were laid out in a randomised block design with three replicates. Hence, image data for a total of 54 trial plots (6 varieties x 3 fungicide treatments x 3 replicates) were captured at four epochs. Data were also captured for a further 60 buffer plots located in between the treatment plots. Each trial plot was approximately 12 m long x 2 m wide. The wheat varieties used were: Calingiri, Corack, Emu Rock, Mace, Magenta and Yitpi. Figure 1 shows the entire trial field observed throughout the study where each colour refers to different fungicide treatments. The total size of the field is approximately 0.3 ha.
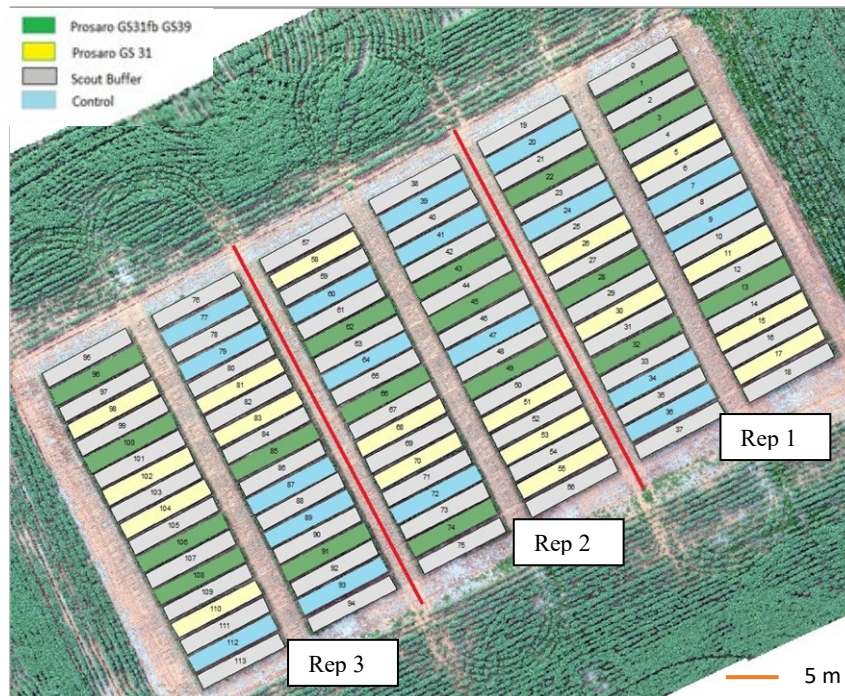
Figure 1: The layout of the study site showing the 54 trial test plots of interest used in this study. Colours (green, yellow and cyan) show the different treatments applied to the plots analysed in this study. The buffer plots, excluded from analysis, are displayed in grey. Rep 1, 2 and 3 refer to the three replicates.

A F550 Flame Wheel by DJI Innovations was used as the sensor platform. The UAV system was built in-house with the specific intention of the ability to cover the study site and allow for easy maintenance. The frame electrics consist of six motors chosen on the principle of redundancy in case of propeller failure. The GNSS navigation unit is a NAZA V2 (DJI) equipped with a compass module powered with LiPO batteries up to 4500mAH capacity. A 2.4 GHZ transmitter controller and Apple iPad were used for directing the UAV across the site and carrying out pre-planned flight missions. The platform has a flight time of approximately 15 minutes. The platform is recommended to be operated in minimal wind speeds (below 10 km/h) to allow for ideal image capturing.

The data capturing commenced in May 2015 immediately after the crop was sown (epoch 0, bare soil), and finished in early October 2015 when the crop was due to be harvested (epoch 4), with three sampling epochs in between (epoch 1, 2, and 3). Multiple sensors were used throughout the project. Initially a GoPro 3+ Silver with a 5.4 mm Flat Lens was chosen as the RGB sensor. The sensor resolution of the GoPro is 10 megapixels. Two other sensors were also used during the study: a Fuji-FinePix X100 and a Canon SX230HS depending on which sensor was available at the time of data capture. Table 1 presents the attributes of the data capture scenarios for the different epochs including effective flight heights, GSDs and front and side overlaps. While a change of the sensors as well as

slightly different flight heights lead to different GSDs and influence the derived CSMs, this did not impact the results of this study because the performance of the three cameras were similar. Furthermore, the sampling epoch interval was sufficiently long so that the crop signal was considerably higher than the accuracy differences among sensors. All epochs with further information are given in Table 1.

Table 1: Data capturing details describing the flight times, dates, heights, Ground Sample Distance GSD, Forward Lap and Side Lap, base to height ratio (B:H) for each epoch, and the camera types and models used at each epoch.

Epoch	Date/Time	Flying height	# images	Camera Type	GSD	Forward Lap	Side Lap	B:H
0	23/05/ 11:00am	17 m	250	GoPro 3+ Silver	0.010 m	90	80	1:2.31
1	04/07/ 10:00am	19 m	128	GoPro 3+ Silver	0.011 m	90	85	1:3.13
2	26/08/ 12:00am	50 m	38	FinePix X100	0.012 m	85	80	1:3.87
3	20/09/ 12:00am	30 m	38	FinePix X100	0.010 m	80	70	1:2.32
4	17/10/ 11:00am	45 m	48	Canon SX230HS	0.014 m	80	80	1:3.46

Originally, 12 GCPs were placed on the bare ground (epoch 0), to generate a dense and accurate ground base model in epoch 0, as the data will be used to generate the base DEM for subsequent epoch growth calculations. As the wheat crops progressed, only six of the GCPs remained visible due to the occlusion from the developing crop canopy. These six GCPs were spread evenly around the trial crop area and were all visible between images captured. The location of all GCPs is provided in Figure 2. The six GCPs were maintained and checked using GNSS RTK before each flight and were always compared back to the original coordinates obtained in epoch 0 to ensure no distortions or errors in the captured data due to GCP movement or disturbance.

5. RESULTS AND DISCUSSION

Four tests were performed to evaluate the results from the five epochs. Firstly, the output of the photogrammetric workflow is evaluated. This was followed by evaluation of the accuracy of the CSMs for each epoch at two different scales: a point-level and plot-level comparison of the CSM heights to GNSS RTK reference heights. Thirdly, the evaluation of the crop growths between epochs was carried out. Finally, the plot-based crop height estimates are examined in relation to vegetation indices derived from multispectral sensors as well as grain yield from the trial plots.

5.1. Assessment of the performance of the photogrammetric workflow

Table 2 shows the Root Mean Square Errors (RMSE) and the re-projection errors generated by the photogrammetric process. The RMSE values are calculated from the ground control points used in the adjustment to generate the CSM (six of which were utilised in each epoch). The re-projection errors were calculated based on the extracted tie-points from the overlapping images. The highest re-projection error of 1.97 pixels occurred in epoch 0. The RMSE of the Z-component of the control for all epochs were very low (Table 2). Even in the case of epoch 1, the RMSE of 0.022 m was only marginally higher than the errors from the manual measurement (tape measure, which is currently the common method of crop height estimation) as well as that of our reference dataset (Z-component of the GNSS RTK) which is 0.016 m (for the control point only). While the horizontal precision is not the primary objective of the comparison in this paper, it should be noted that the values for RMSE in this case for epoch 0 and 1 are significantly higher than for the other epochs. This is due to the camera used (GoPro 3+ Silver), and the lens distortions associated with it. For this camera, the lens distortion model could not sufficiently compensate for the actual errors due to lens distortion for such cameras.

**Table 2: Re-projection error and RMSE values for each epoch and coordinates.**

	Epoch 0	Epoch 1	Epoch 2	Epoch 3	Epoch 4
re-projection error [pix]	1.97	1.17	0.798	1.17	1.64
Nº tie points	541,153	350,957	107,981	60,514	239,154
Nº projections	2,877,140	1,091,790	321,006	149,637	723,136
RMSE X [m]	0.051	0.063	0.007	0.007	0.010
RMSE Y [m]	0.069	0.079	0.005	0.006	0.006
RMSE Z [m]	0.003	0.022	0.002	0.005	0.005
RMSE [m]	0.086	0.103	0.009	0.010	0.013

5.2 Comparison of absolute crop height estimates from the CSM and GNSS in each epoch

5.2.1. Point-based comparison

For the reference GNSS RTK data, observations were taken at intervals along the centreline of each plot (shown in Figure 2). The average number of points taken were between 2 and 3 for each plot over the different epochs. The height at the same locations of the GNSS RTK were extracted from the CSMs, using the GNSS RTK coordinates to index into the calculated CSM and retrieve the height values at these locations. These extracted values were then compared to the GNSS RTK observations. Large discrepancies between the CSM and GNSS RTK values were removed where these fell outside of threshold values (<-0.35 m or > +0.35 m). The thresholds were defined at 30% of crop target

28

heights for affected epochs. The highest number of these values were eliminated in epoch 3 (80) and epoch 4 (25) due to windy conditions which forced the crop to move, and biased the resulting heights. The results are summarised in Table 3; the number of paired observations varied between epochs due partly to the removal of different numbers of outliers from the datasets, and partly to varying number of observations per plot taken at different epochs.
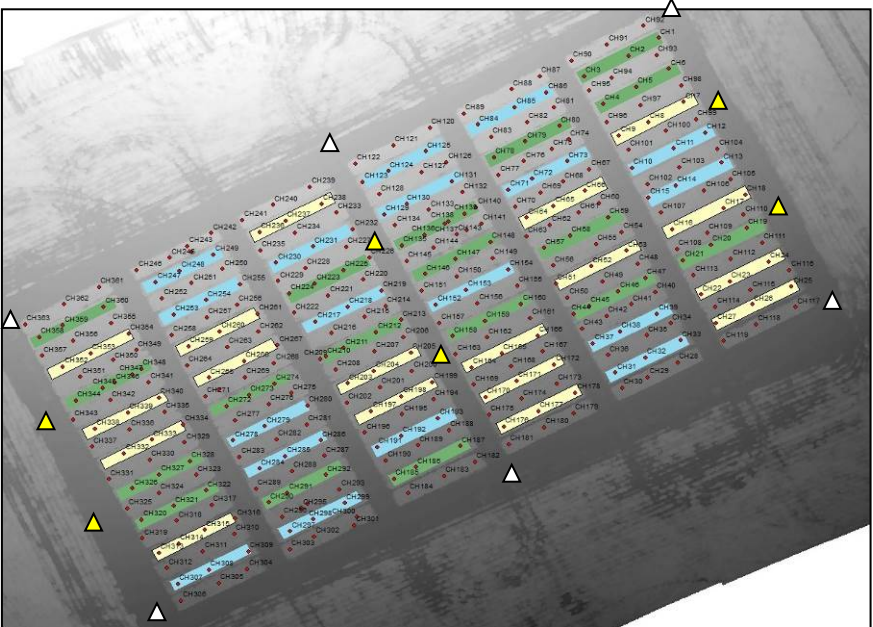

Figure 2: DSM with 363 GNSS RTK reference observations (dots in plots) for epoch 4; triangles indicate the location of the GCPs.

Table 3: Comparison of CSM extracted points to GNSS RTK reference points for each epoch. Note that sample sizes vary between epochs (except for epochs 0 and 1), due to removal of outlier points affected by crop movement from wind gusts. Please note that at epochs 0 and 1, on average two observations were recorded per plot, whereas all the other epochs had on average three observations per plot.

Epoch	# of reference points (total # observed)	Average bias	p-value	RMSE
0	239 (239)	+0.080m	0.131	0.088 m
1	239 (239)	-0.108m	0.053	0.119 m
2	301 (301)	-0.088m	0.080	0.119 m
3	278 (358)	+0.021m	0.644	0.175 m
4	312 (337)	-0.100m	0.042	0.136 m

Comparison of the GNSS RTK and CSM/DSM results for each epoch were evaluated with a two-tailed two-sample t-test with equal variance assumption, because variances between the two methods

were homogeneous. The results showed that the CSM and the GNSS RTK produce comparable height estimates ($p > 0.05$) except at epoch 4, which showed a marginal difference (Table 3). The RMSE represents the root mean square of the differences between absolute heights for CSM and GNSS across all plots. It shows that the variability between CSM and GNSS heights for all plots remains consistent across all epochs. It is not the error between each measurement. For further analyses, box plots of the paired-point absolute heights differences between DSM/CSM and GNSS are shown to help visualise systematic bias at each epoch (Figure 3). Epoch 0, has the narrowest interquartile range, indicating little variation between the CSM and GNSS RTK heights. The dispersion of data is only slightly higher for the first, second and fourth epoch. However, the average differences between the CSM heights and the GNSS reference observations were generally no more than 10 cm (Table 3). From the boxplots in Figure 3, it can also be observed that epoch 3 demonstrates a greater dispersion than the other epochs. The reasons for this are explored in the following section. It should also be noted that the outlier magnitudes for epoch 3 lay outside the visible range of values presented in Figure 3 (hence they are not visible in this plot as many are in excess of 1 m). This is likely to be due to high localised variability in the crop growth evident in Figure 9 (for example, note the red band of plots in the middle of columns 4-6 in panel b), as well as the presence of wind during the data capture.
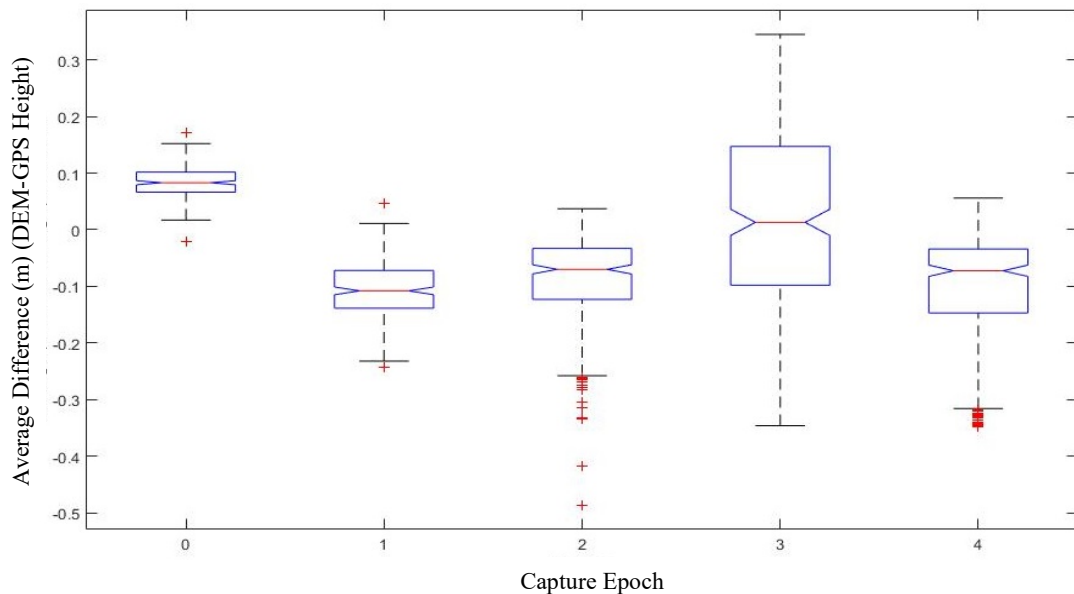
Figure 3: Box plots of the absolute height differences between paired DSM/CSM and GNSS RTK heights at each epoch The red line represents the median value, the extents of the blue boxes represents the 1st and third quartiles (q1 and q3 respectively). The upper whiskers represent the q3 + 1.5*interquartile range, and the lower represents q1 – 1.5*interquartile range. The red crosses denoted data outside these limits.

Expanding on the points mentioned above, the following conclusions are made as to why the DSM of epoch 0 and 3 were slightly higher than the reference GNSS observations. Epoch 0 was the first epoch flown to generate a bare ground Digital Surface Model (DSM) where all other epochs can be

subtracted from to determine the change in growth. However, being just bare soil it was influenced by other factors in close proximity to the ground, for example, the stubble left over from the previous year's harvest. Figure 4 displays some potential areas of interest where the true ground height may not have been computed exactly due to some stubble residue. Although the reference data capturing and UAV flights took place only days after the crops were seeded, it was realised the stubble from the previous harvest could create a positive bias when determining the exact ground base DSM. It is concluded that the DSM of epoch 0 was on average higher than the reference observations due to the mismatch of the DSM generated stubble spikes to the GNSS RTK ground observation.
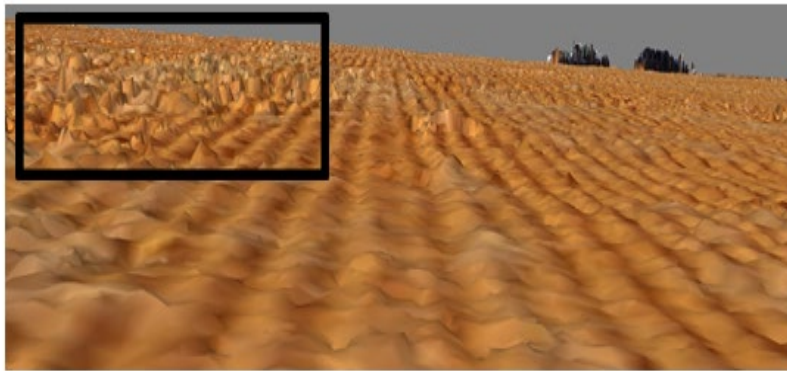
Figure 4: Close up of epoch 0, and illustration of the potential issues that arise from stubble of previous crops on accurate determination of DSM.

The bias of all other captured data can be also explained with the image matching process. For example, not all points in the CSM will be at the head heights of the wheat crop, i.e. instead of matching points on the head height, lower parts such as the leaves of the crops are captured (Figure 5). Some of those points may also be capturing areas towards the base of the crop and potentially at the ground level in some instances (depending on the density of the plants). Hence, if there are many leaves and when those leaves are furthest away from the heads (epoch 3) then the bias has to be negative. Therefore, if there are not enough common points at the head level of the crops, the height can actually be missed and cause a dip in the CSM as it joins lower points to higher points. Similar results were found by Anthony, et al. (2014) when they measured corn heights using LiDAR and a Laser Scanner mounted to a UAV.

Figure 5: Illustration of potential source of CSM inaccuracy based on image matching.

A problem arose with processing of epoch 3 imagery. Crop imagery at this epoch was captured under less than ideal conditions. Wind gusts above 30 km/h buffeted the crop at the time of image capture, causing a movement in the crop canopy. As the UAV made one pass or strip down the site, it would take images every two seconds and capture the exact location of the top of the wheat crops at that point in time. However, on the returning adjacent pass when capturing the overlap image of the same location, the top of the wheat crops had blown in another direction, therefore changing the positon of the plant. This problem displays itself in the boxplot in Figure 3, where a large number of outliers are highlighted for epoch 3. Figure 6 displays a close up of the 3D model of the crop canopy generated from the data captured under the prevailing wind conditions; revealing that no crop height could be generated from the imagery in areas affected severely by wind at the time of data capture.
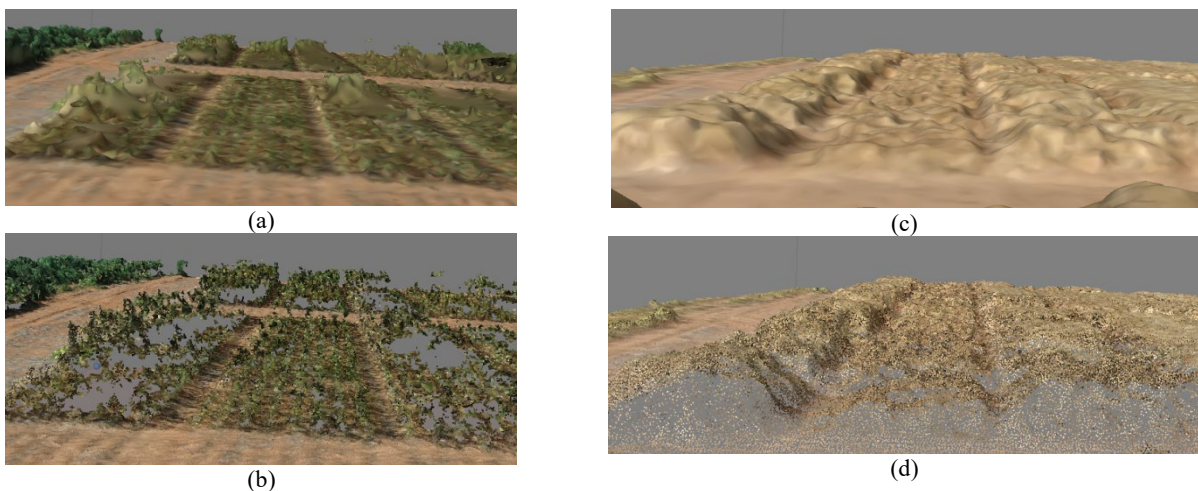

Figure 6: Illustration of mismatching in epoch 3 due to wind conditions (a). (a) shows the mesh and (b) the point cloud from epoch 3. This is contrasted to epoch 4's mesh (c) and its point cloud (d).

5.2.2 Plot-Based Comparison

For the plot-wise comparison, the average absolute height of the crop in a plot using the photogrammetric CSM data are compared with the average GNSS RTK observations (Figure 7). The plot boundaries were created with a 0.3 m buffer from the edge of the crops to minimise edge effects. A threshold of 10 cm was set, with any differences outside this range being flagged as gross error and therefore eliminated. Figure 7 further illustrates that the two methods give highly comparable absolute height estimates. For epoch 3 and to a lesser extent epoch 4, however, GNSS heights showed slight bias (underestimation), consistent with results shown in Fig 3.
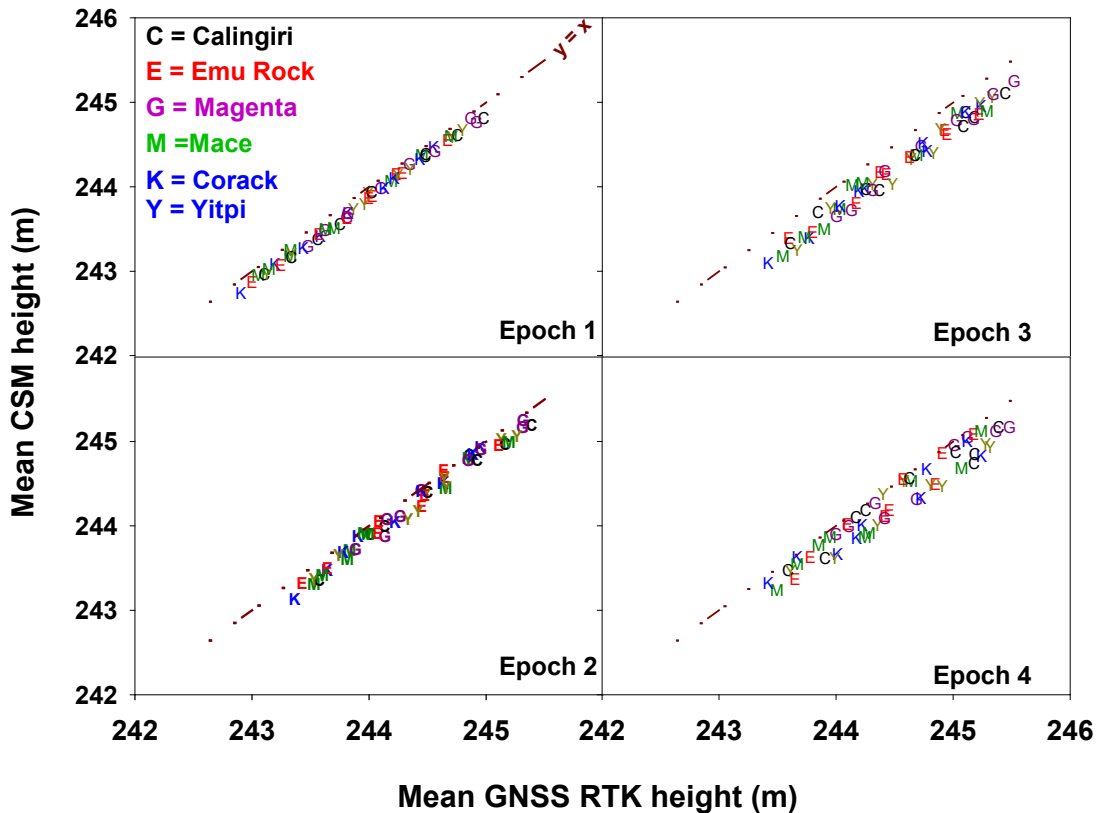

Figure 7: Comparison of absolute height measurement techniques based on plot-average height estimates for different wheat varieties at different epochs. Each point denotes average crop height estimate per plot. The y = x is a line parity between the two methods under comparison.

5.3 Evaluation of the relative crop height between epochs

Changes in crop height were evaluated at the plot level. The relative crop heights were determined as the differences between epoch t_i and epoch t_0 (i.e. the bare ground) over the interpolated surfaces. This was conducted to evaluate whether the CSMs derived from images captured on a UVA platform can be used to determine temporal changes in crop height. The results are presented in Figure 8.

It is readily observable that the crop varieties differ in their height. For the most part, the crop height estimates from UAV imagery effectively reproduced/reflected the expected height rankings of the varieties used in this study, demonstrating the suitability of the technology for crop height growth monitoring.
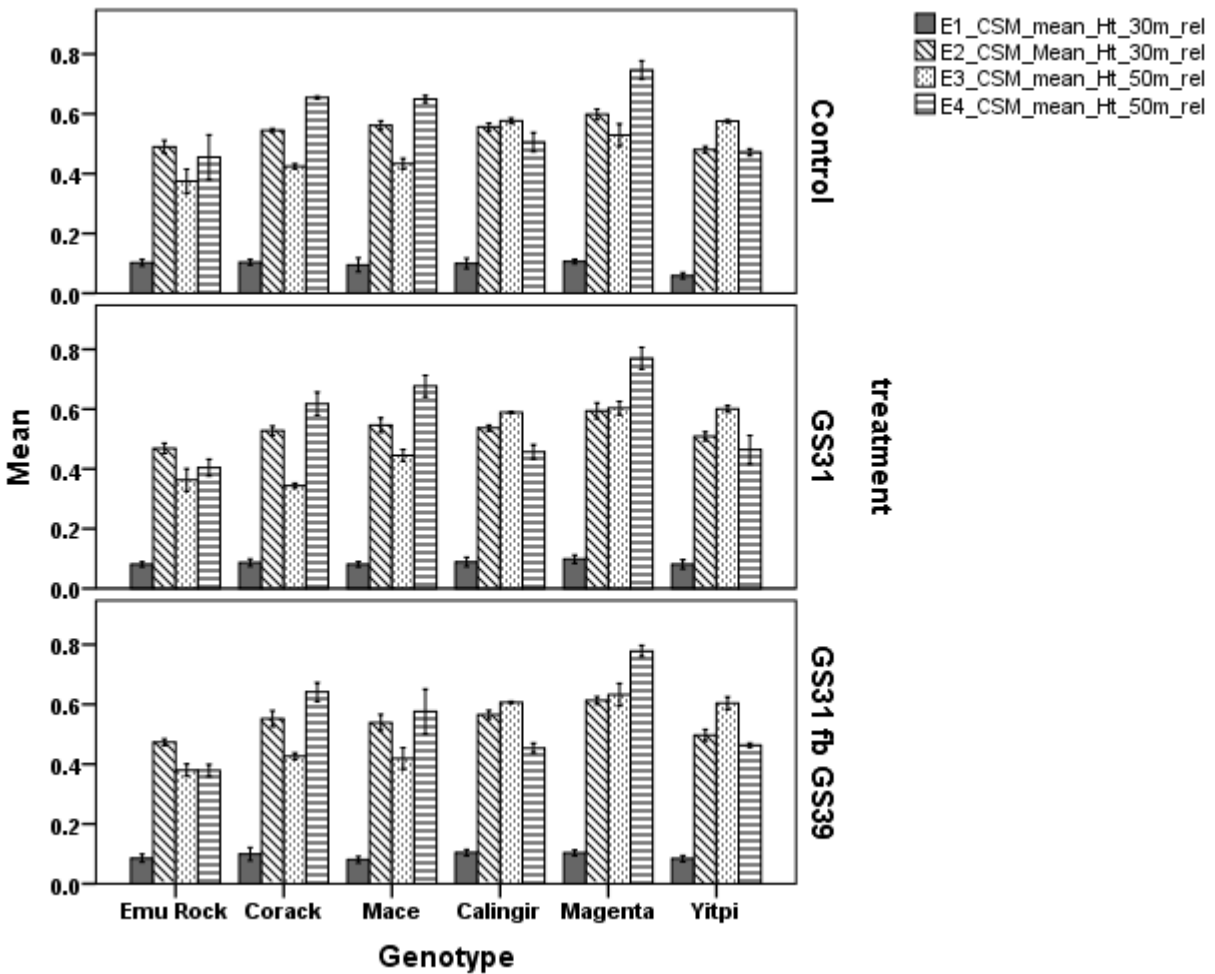
Figure 8: Mean relative crop heights at different epochs estimated as the difference between heights at epoch *i* less the corresponding heights at epoch *0*. For each crop variety and fungicide treatments, data shown are mean heights ± 1 standard error (over 3 replicated plots). For epochs 1 and 2 (E1, E2) imagery was captured from 30 m height; for the rest from 50 m. Top panel represents plots that received no fungicide treatment (Control plots); middle panel for plots that received treatment at GS31; bottom panel is for plots which were treated with fungicide at GS31 followed by at GS39.

The largest change in crop height was observed between epochs 1 to 2 for all varieties (Fig. 8, 9). These two epochs represent the period between 7 July and 26 August. For Western Australia, these are the months of winter, and the highest rainfall period. The large growth between the epochs can also be justified by the 50 days interval between the two epochs, allowing for a longer duration for the crops to grow. During this period, the crops progressed from late tillering through stem extension

and to flowering developmental stages (depending on variety) when most of the extension growth occurs.

The next largest growth changes occurred between E_0 and E_1 which had a duration of 45 days, between 23 May and 7 July. This was the initial growing period from sowing (bare ground) to early/ mid-tillering growth stages, and so it was expected for it to be ranked as the second largest growth change between epochs. However, despite the long duration, the magnitude of growth between E_0 and E_1 was less than that between E_1 and E_2 because for part of the time the crop did not emerge, and that the crop growth during the establishment phase is naturally slow.

(a)

(b)

(c)

(d)
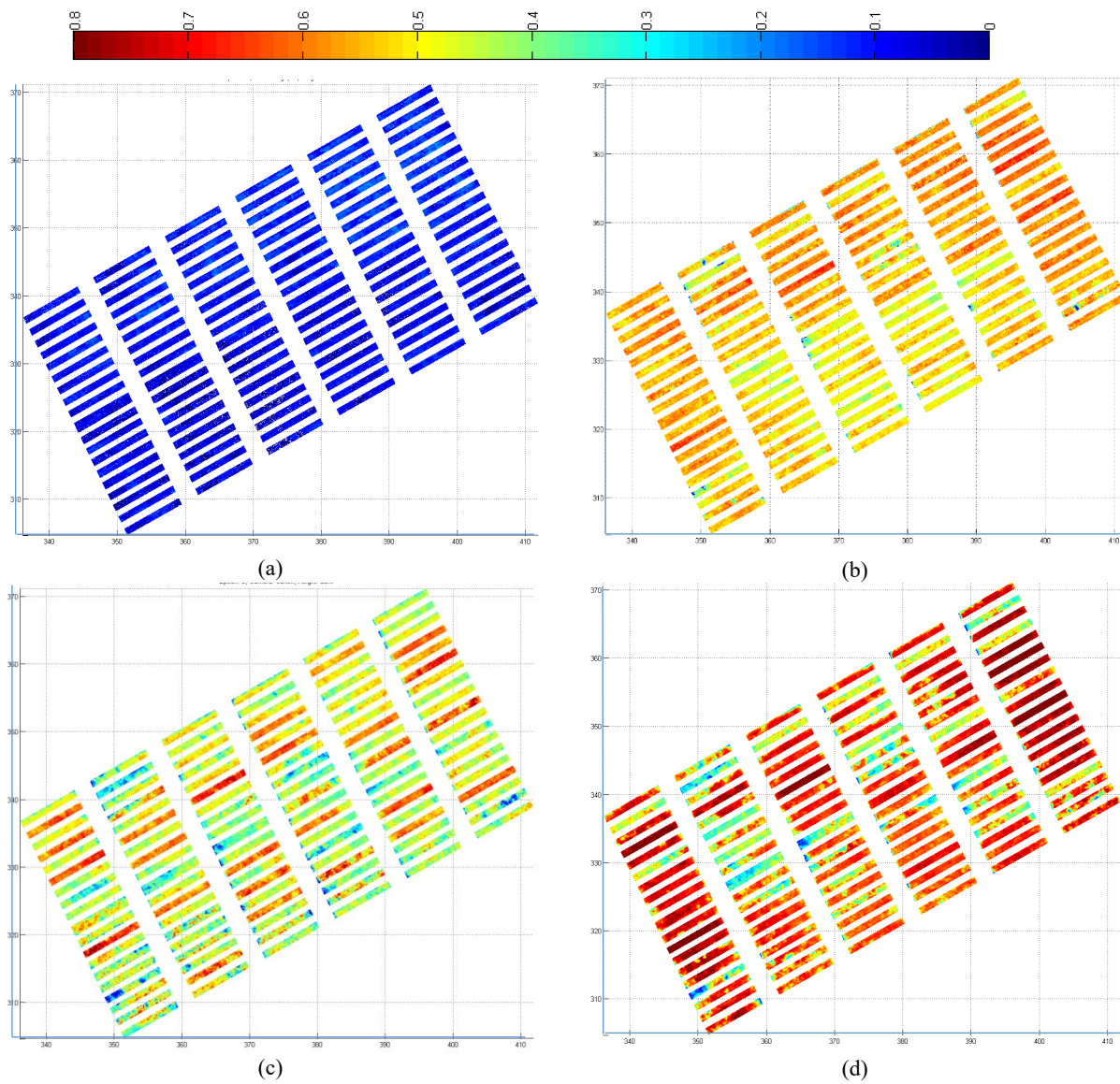
Figure 9. Temporal patterns in crop heights determined from UAV-imagery. Eastings (x axis) have been shifted by 471000 m and northings (y axis) by 6489000 m from their raw MGA zone 50 coordinate system. The plots (a),

(b), (c) and (d) represent the difference between epoch 1, epoch 2, epoch 3 and epoch 4 to the bare ground (epoch 0), respectively.

The interval between epochs 2 and 3 fell during the winter to spring transition (August 26th to September 20th). Although the duration between these epochs was 25 days with favourable temperatures for crop growth, only a modest height growth was expected since stem extension is largely complete by this time, and height increases are likely to accrue from ear growth, which has a considerably smaller size than the stem.

Finally, the last growth period to be measured (epoch 3 to 4) is also when the smallest amount of growth occurred. These are the dates from 20 September to 7 October when soil moisture supply drops rapidly, weather is warming and crops are in the grain filling phase. As expected, this growth period had the least amount of height change as the crop heads began to droop, at least for some varieties (Yitpi and Calingiri).

Of all 54 plots monitored four times (i.e., 216 observations), two major outliers were apparent from the temporal analysis of crop height growth. These were consecutive observations from one Calingiri plot in replicate 3. Examination of these outlies revealed inconsistency between observations captured at epochs 2 and 3, which caused incorrectly large crop height growth estimates. Further examination highlighted the crops were severely distorted by wind during image capture, thus introducing large spikes in the CSMs generated from these epochs, as also described earlier.

An interesting observation is that at E_3, the effect of canopy movement due to wind had different influences on crop height estimates. For the short stature varieties (Emu Rock, Corack and Mace), which at E_2 were close to their maximum heights, wind movement of the canopy caused the height estimates at E_3 to appear less than the respective estimates at E_2 (Fig. 8). By contrast, for the taller varieties (Calingiri, Yitpi and Magenta), which at E_2 were well below their peak height, the wind did not cause a dip in the crop height estimates at E_3 relative to the E_2 estimates because the height growth between E_2 and E_3 was large enough to offset the wind induced underestimation.

Overall, these results indicate that a detailed analysis of the different varieties, and changes in their heights or growth rate, as well as the absolute height can be derived using CSM generated from UAV captured imagery. This is of course dependent on weather and flight conditions, as well as factors affecting the construction of the CSM, such as the GCP distribution. These factors can normally affect

the results adversely, and in many cases cause underestimation of heights. With proper accounting of these potential pitfalls, however, it is suggested that the CSM derived crop height can be used for monitoring crop growth in wheat varieties with contrasting statures. It is also useful for revealing spatial variation in crop height and as a proxy crop biomass.

5.4. Correlation of CSM relative heights with yield and NDVI

For the trial plots, multispectral data (green, red, red-edge and near infrared) were collected from early July to late September overlapping the UAV imagery epochs. Additionally, crop yields were measured for all plots. Normalised difference vegetation index (NDVI) and yield data were examined in relation to the height estimates from the UAV imagery to explore how well the height data relate to crop density and yield data (Figure 10). The analyses showed that plot level crop height estimates (variable IDs 2-5) were weakly related to crop yield (variable ID 1), as would generally be expected. Crop height is usually better correlated with crop total biomass or density. Accordingly, the CSM crop heights (variable IDs 2-5) were generally positively correlated with crop NDVI estimates (variable IDs 6-15), which are proxies for crop density and/or biomass. The correlations were stronger for NDVI measures captured closer to the dates of UVA height capture epochs (e.g., E4 and E5 vs NDVI estimates from 26 Aug to 23 Sep; or E2 heights vs NDVI estimates during 22 July to 12 Aug). Conversely, NDVI and crop height estimates that were captured further apart in time were either weakly, or negatively correlated (e.g. correlations between height estimates at epoch 2 and NDVI estimates during 02 - 23 Sep, i.e., variable IDs 12-15, were negative). Collectively, these results suggest that while there is a modest to strong association between independent estimates of crop height and vegetation indices, this does not appar to extend to crop yield or at best the correlation is weak. A demonstration of existence of a strong correlation can potentially be useful for prediction of crop yield from remotely sensed height estimates; it thus worth further investigating whether this holds under different environemntal stress conditions that can affect crop height and yield.
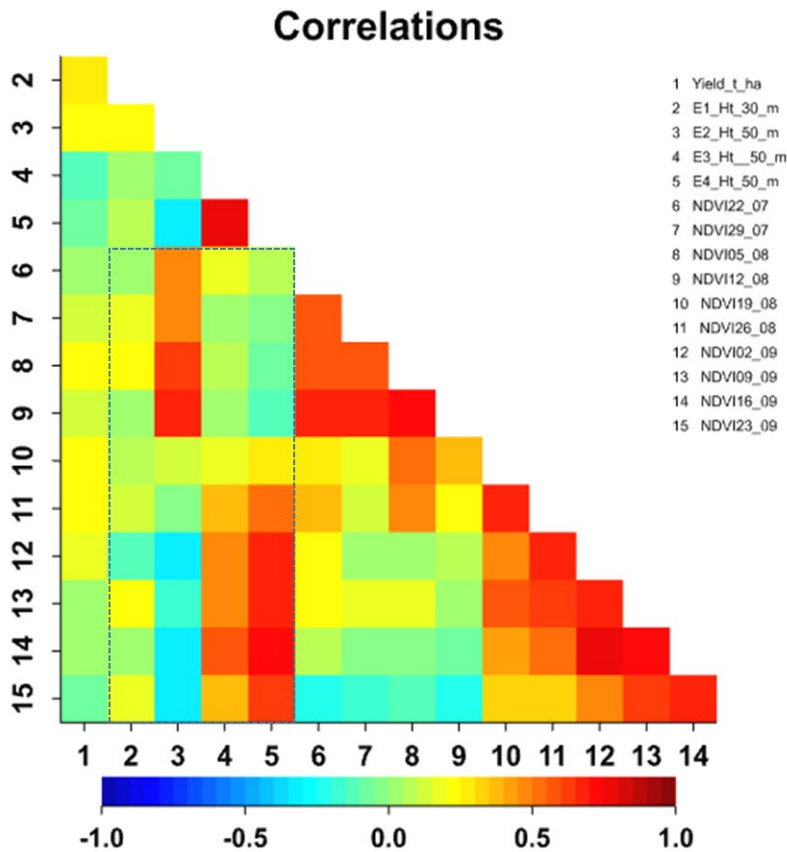
Figure 10. Correlations of plot level height estimates (variables 2-5) with crop yield (variable 1) as well as with normalised difference vegetation indices (RRed-RNIR)/(RRed+RNIR) from 22 July to 23 September (variables 6 – 15, respectively) highlighted by the dashed rectangle.

6. CONCLUSIONS

The data and information attained from the CSMs at each epoch, on the whole, are acceptable and do reflect realistic crop height information. However, the CSMs tended to slightly underestimate crop height compared to observed reference data. Thus, there is a potential for further investigation for correction of biases in the CSM heights.

Nonetheless, the CSM methodology was sufficiently robust for detecting changes in crop/canopy height, and as such, it is useful for quantitative as well as qualitative monitoring purpose. As a result, it was possible to detect growth differences between epochs, and between wheat varieties with contrasting heights. If applied treatments were to cause height growth differences, the evidence from this study suggests that CSMs generated from images captured on UAV-borne consumer grade camera could provide sufficient information to detect crop/canopy height growth differences due to management practices. The disease management practice (fungicide treatments) used here, however,

was not expected to affect crop height. Hence, the absence of a demonstrable fungicide treatment effect on crop height does not invalidate the capability of the technology.

During the processing of the results, important limitations were noticed mainly from the influence of weather. The weather conditions, also noted by Bendig et al. (2013), imposed restrictions on the ability of flying and capturing data in windy conditions.

On the whole, the results from this work demonstrate a successful utilisation of UAVs in the agriculture industry. In particular, deployment of protocols for creation of 3D models when supplemented with additional sensor data such as that from Near Infar-Red (NIR) imagery provides opportunity for extraction of detailed cropping information for particular areas of interest.

While our research so far was limited to geometric features of the crops (CSM/crop height), recent publications show that diseases or treatments of corps can be also detected using spectral information such as the NDVI (e.g. Nebiker et al., 2016). Therefore, the next step is to include spectral information into the analysis. A thorough evaluation of which features contribute significantly to the best classification result will be part of the studies.

REFERENCES

Abbasi, M., Darvishsefat, A. A., & Schaepman, M. E. (2010). Spectral reflectance of rice canopy and Red Edge Position (REP) as indicator of high-yielding variety. *ISPRS Archives*, XXXVIII-B7. 1-5

Anthony, D., Elbaum, S., Lorenz, A., & Detweiler, C. (2014). On crop height estimation with UAVs. In *2014 IEEE/RSJ International Conference on Intelligent Robots and Systems (IROS 2014)* 4805-4812.

Batzdorfer, S., Bobbe, M., Becker, M., Harms, H., & Bestmann, U. (2017). Multisensor equipped uav/ugv for automated exploration. *ISPRS Archives*, XLII-2/W6, 33-40.

Bendig, J., Bolten, A., & Bareth, G. (2013). UAV-based imaging for multi-temporal, very high resolution crop surface models to monitor crop growth variability. *Photogrammetrie-Fernerkundung-Geoinformation*, 2013/6, 551-562.

Boon, M. A., Drijfhout, A. P., & Tesfamichael, S. (2017). Comparison of a fixed-wing and multi-rotor UAV for environmental mapping applications: A Case Study. *ISPRS Archives*, XLII-2/W6, 47-54.

Candare, R. J., Japitana, M., Cubillas, J. E., & Ramirez, C. B. (2016). Mapping of high value crops through an object-based SVM model using lidar data and orthophoto in Agusan del Norte Philippines. *ISPRS Annals*, III-7, 165-172.

Chiabrando, F., & Losè, L. T. (2017). Performance evaluation of COTS UAV for architectural heritage documentation. A test on S. Giuliano chapel in Savigliano (CN)–Italy. *ISPRS Archives*, XLII-2/W6, 77-84.

Colomina, I., & Molina, P. (2014). Unmanned aerial systems for photogrammetry and remote sensing: A review. *ISPRS Journal of photogrammetry and remote sensing*, 92, 79-97

Duarte, D., Nex, F., Kerle, N., & Vosselman, G. (2017). Towards a more efficient detection of earthquake induced façade damages using oblique UAV imagery. *ISPRS Archives*, XLII-2/W6, 93-100.

Eisenbeiss, H. (2008). UAV photogrammetry in plant sciences and geology. In *6th ARIDA Workshop on Innovations in 3D Measurement, Modeling and Visualization*, Povo (Trento), Italy.

Geipel, J., Link, J., & Claupein, W. (2014). Combined spectral and spatial modeling of corn yield based on aerial images and crop surface models acquired with an unmanned aircraft system. *Remote Sensing*, 6(11), 10335-10355.

Goyne, P. J., Meinke, H., Milroy, S. P., Hammer, G. L., & Hare, J. M. (1996). Development and use of a barley crop simulation model to evaluate production management strategies in north-eastern Australia. *Australian Journal of Agricultural Research*, 47(7), 997-1015.

Herrmann, I., Pimstein, A., Karnieli, A., Cohen, Y., Alchanatis, V., & Bonfi, J. D. (2010). Utilising the VENμS Red Edge bands for assessing LAI in crop fields. *ISPRS Archives* XXXVIII-4-8-2-W9: 34-39.

Hese, S., & Behrendt, F. (2017). Multiseasonal Tree Crown Structure Mapping with Point Clouds from OTS Quadrocopter Systems. *ISPRS Archives*, XLII-2/W6, 141-143.

Kraus, K., (2007). Photogrammetry: Geometry from Images and Laser Scans. *Walter de Gruyter (1807)*, ASIN: B01FIZ8L6G, 459 pages.

Laudien, R., & Bareth, G. (2006). Multitemporal hyperspectral data analysis for regional detection of plant diseases by using a tractor-and an airborne-based spectrometer. *Photogrammetrie Fernerkundung Geoinformation*, 2006/3, 217-227.

Maurer, M., Hofer, M., Fraundorfer, F., & Bischof, H. (2017). Automated inspection of power line corridors to measure vegetation undercut using UAV-based images. *ISPRS Annals*, IV-2/W3, 33-40.

Mostafa, M. R. (2017). Accuracy assessment of professional grade unmanned systems for high precision airborne mapping. *ISPRS Archives*, XLII-2/W6, 257-261.

Mulla, D. J. (2013). Twenty five years of remote sensing in precision agriculture: Key advances and remaining knowledge gaps. *Biosystems engineering*, 114(4), 358-371.

Nebiker, S., Lack, N., Abächerli, M., & Läderach, S. (2016). Light-weight multispectral UAV sensors and their capabilities for predicting grain yield and detecting plant diseases. *ISPRS Archives*, XLI-B1, 963–970.

Rehak, M., & Skaloud, J. (2017). Performance assessment of integrated sensor orientation with a low-cost GNSS receiver. *ISPRS Annals*, IV-2/W3, 75-80.

Shi, S., Gong, W., Du, L., Sun, J., & Yang, J. (2016). Potential application of novel hyperspectral lidar for monitoring crops nitrogen stress. *ISPRS Archives*, XLI-B8, 1043-1047.

Sona, G., Passoni, D., Pinto, L., Pagliari, D., Masseroni, D., Ortuani, B., & Facchi, A. (2016). UAV multispectral survey to map soil and crop for precision farming applications. *ISPRS Archives*, Volume XLI-B1, 2016, 1023–1029.

Stöcker, C., Nex, F., Koeva, M., & Gerke, M. (2017). Quality assessment of combined IMU/GNSS data for direct georeferencing in the context of UAV-based mapping. *ISPRS Archives*, 42, XLII-2/W6, 355-361

St-Onge, B., Vega, C., Fournier, R. A., & Hu, Y. (2008). Mapping canopy height using a combination of digital stereo-photogrammetry and lidar. *International Journal of Remote Sensing*, 29(11), 3343-3364.

Taddia, Y., Corbau, C., Zambello, E., Russo, V., Simeoni, U., Russo, P., & Pellegrinelli, A. (2017). UAVs to assess the evolution of embryo dunes. *ISPRS Archives*, XLII-2/W6, 363-369.

Wang, Y., Liao, Q., Yang, G., Feng, H., Yang, X., & Yue, J. (2016). Comparing broad-band and red edge-based spectral vegetation indices to estimate nitrogen concentration of crops using casi data. *ISPRS Archives*, XLI-B7, 137-143